

# NANOPROBE RESULTS: METROLOGY & CONTROL IN STACKED CLOSED-LOOP SYSTEMS

C. Engblom\*, Y.M. Abiven, F. Alves, N. Jobert, F. Langlois, A. Lestrade, S. Kubsky,  
Synchrotron SOLEIL, Saint-Aubin, France  
T. Stankevič, MAXIV, Lund, Sweden

## Abstract

Over the course of four years, the Nanoprobe project worked to deliver prototypes capable of nm-precision and accuracy with long-range millimetric sample positioning in 3D- scanning tomography for long beamline endstations of Synchrotron Soleil and MAXIV. The ambition of the project necessitated a joint progress between several fields of expertise combining mechanics, metrology, motion control, and software programming. Interferometry in stage characterization has been a crucial point; not only to qualify motion errors but to actively integrate it into control systems with feedback and/or feedforward schemes in order to reduce XYZ position errors down to the nm- level. As such, a new way of characterizing rotation stages [1] [2] was developed and ultimately used in control schemes utilising the Delta Tau PowerPMAC platform [3] [4]. This paper details the obtained results as well as the methodology and approach of the project to achieve this.

## INTRODUCTION & APPROACH

The Nanoprobe Project was initiated to deliver a scanning hard X-ray double Fresnel Zone Plate (FZP)- based microscope with a scanning sample stage for long beamline endstations in Nanoscopium [5] of Synchrotron Soleil and NanoMAX [6] of MAXIV. Some of the challenging aspects were to produce nanometric XYZ resolutions coupled with deca-millimeter range with 360° sample movement and rotation while also providing step-scans, Flyscans [7], and long-term stability. Figure 1 shows a schematic of the end-station setup with beam focusing stages (Fresnel Zone Plates, Central Stop, Order Sorting Aperture) and Sample Stage. The approach was, in addition of providing a stable environment in terms of vibration and thermals, to construct a modular and stacked design with an interferometric feedback system and the possibility of using position compensation (in feedforward control) to diminish repeatable errors. Interferometry was therefore not only used for feedback but also in measuring and characterizing stages to determine repeatable and non-repeatable errors. This paper will focus on the setup and evaluation of the sample- and FZP stages as these were the most challenging in terms of positioning stability and multi-axis synchronization.

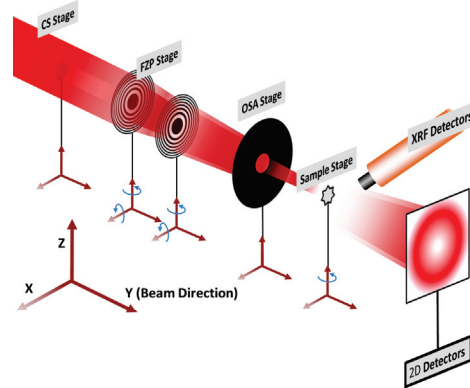


Figure 1: End-station scheme and XYZ- orientation of stages and detectors in respect to beam; each stage has its degrees of freedom (DOF) marked out.

## SYSTEM OVERVIEW

### Environment

The prototype was mounted, tested, and characterized in a thermally stabilized environment. Figure 2 shows the prototype environment; a marble table placed in a climate controlled room. The marble table itself was insulated in such a way to minimize XY-gradients (and thus XY- positionally induced thermal drifts), with water circulation and system enclosure to add for thermal impedance.



Figure 2: The system in a thermally stabilized environment; here with an insulated granite table, water circulation and system enclosure.

### Sample Stage

The sample stage was, as seen in Fig. 1, tasked to move the sample in 4 degrees of freedom (DOF). The XYZ-space (Y being the beam direction) was to be scanned with nanometer

\* christer.engblom@synchrotron-soleil.fr

resolution over deca-mm course, while the Rz-rotation was done with  $\mu\text{rad}$  resolution with a full  $360^\circ$  range.

Figure 3 shows the setup of the sample stage, here with six positional drives including two that were used for sample alignment on the Rz-rotational drive. The X-axis was to be used mainly for continuous scanning while the Y-, Z-, and Rz- axes were used for step scans. The sample holder (#6 in Fig. 3) also acted as a reflector to be used for interferometric sample tracking: ideally a cylindrical shape (to allow for rotational movements), but occasionally chosen to be a cubic reflector when only characterizing linear XYZ- movements. The sample rotational drive, small and lightweight (and piezo- driven), was to be used with interferometry for characterization with/or feedback to reduce any movement errors caused by the rotation stage.

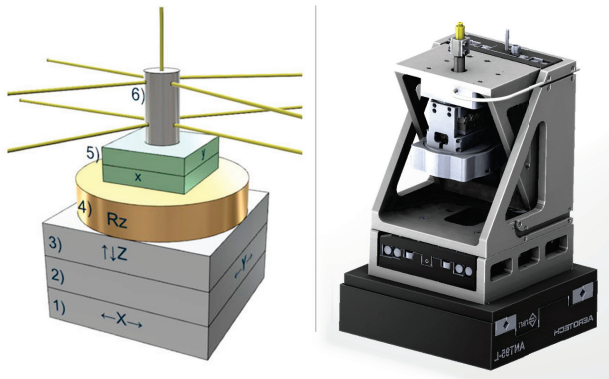


Figure 3: The sample stage. *Left:* schematic diagram illustrating the positioners and their respective directions. (1) X-axis, for continuous scanning. (2) Y-Axis (beam), piezo driven positioner for stepruns. (3) Z-Axis, piezo driven positioner for stepruns. (4) Rz-Axis, rotary piezo driven positioner for stepruns. (5) XY-Axes, piezo driven positioner for sample alignment. (6) Sample holder and interferometer reflector (in this case, cylindrical). Yellow lines depict interferometry beams that are used for sample tracking. *Right:* Mechanical drawing of the stage.

### Sample Stage Control

Figure 4 illustrates the sample stage cascaded control scheme with a high-frequency inner control-loop residing in the actuator driver, and a lower-frequency outer loop containing a Delta Tau [4] controller (Soleil high-end controller from the REVOLUTION project [3]). Motion errors of the positional drives were reduced by two approaches:

- Position compensation:* repeatable errors were measured and corrected for in a feedforward manner. This approach needed interferometry for creating the compensation table; these errors would be corrected and reduced by using all available positional drives (effectively using multi- axial error correction). Interferometry is only used for error mapping; no interferometry is necessarily needed during on-line use (ex. beamlines).
- Interferometry feedback:* closed- loop control with interferometry feedback at the Delta Tau controller level.

Interferometry measurements were done very close to the sample (on sample holder reflector, see #6 in Fig. 3) providing the means to correct for repeatable and non-repeatable errors. Note: Assuming a perfect reflector, any perceived error is the actual position error. If not the case, aka imperfect reflector, reflector surface mapping is essential for position compensation on the interferometry signal.

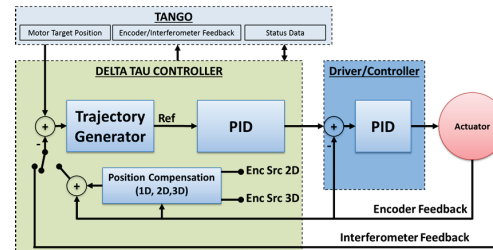


Figure 4: Sample stage control scheme; cascaded with inner loop done at positioner driver level and outer loop with a Delta Tau controller. Position error table compensation and interferometry feedback loop done at Delta Tau controller level. TANGO-Delta Tau interfacing done via ethernet.

### FZP Stage

This stage, see Fig. 5, consists of two identical and symmetric modules that each hold a fresnel zone plate. Each module has five DOF which allows for translations in XYZ- space, as well as tilting in the Rx and Rz rotational space. All positional drives are of piezo stick-and-slip type, allowing for high-resolution and long travel range. In addition, each module is equipped with interferometry sensors which provides (X,Z,Rx,Rz)- feedback.

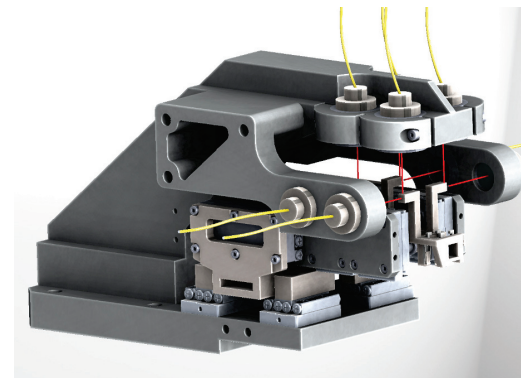


Figure 5: Mechanical drawing of the full FZP stage with the eight interferometer sensor heads with fiberoptics (marked green). Interferometry beams are marked red.

### FZP Stage Control

Figure 6 shows the cascaded FZP control scheme where the high-frequency inner loop was handled by the driver/controller of the positioner, and the slower outer control loop was handled with interferometry as feedback via TANGO/Galil [8] control. The FZP was controlled using higher-level coding (Python) to perform complex motion

with interferometry as feedback; kinematic equations were implemented within a python environment and all motion commands and interferometry/encoder feedback were communicated to the positioner to/from the TANGO device as depicted in Fig. 6. The outermost TANGO/Galil control loop was made to compensate for slow drifts at corrections rates of  $<\sim 1\text{Hz}$  which is why this particular setup works well with static positioning such as the FZP, CS, and OSA stages.

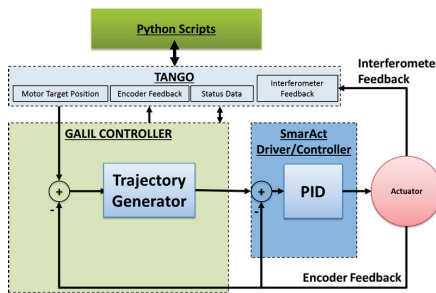


Figure 6: FZP stage control scheme; cascaded with inner loop done at positioner driver level and outer loop with Galil/TANGO control. Interferometry feedback loop and kinematic conversions done at TANGO level with Python scripts.

## RESULTS

### Environment Stability

Better than  $1mK$  resolution (at  $1000mK$  intervals) temperature measurements were performed of which the environment (marble table, inside enclosure) was thermally assessed to have drifts below  $10mK$  (which in this case would result in  $\sim 10\text{nm}$  positional drifts) over an 8-hour period (see Fig. 7). The marble insulation proved successful as the XY- temperature gradients were extremely low.



Figure 7: Relative temperature drifts for the individual sensors placed in/on the marble table for the endstation prototype during an 8-hour span; all sensors drift less than  $10mK$ .

### Sample Stage Motion Errors

Actuation motion errors is a challenge with nanopositioning systems as all positional trajectories will exhibit

in-axis or out-of-axis (aka parasitic) motion errors. Figures 8 and 9 shows two examples of where the X-axis motion errors were measured using interferometry during X- and Z- scans over the course of  $2\text{mm}$ . In the case of Fig. 8, the X-errors during X-axis movements were highly repeatable; making it viable to be corrected for by using approach 1 and 2 listed in subsection *Sample Stage Control*. Figure 9 exhibit non-repeatable periodic errors on the X-axis (had similar non-repeatable errors in the Z-axis) during Z-axis movements making approach 2 listed in subsection *Sample Stage Control* the feasible choice.

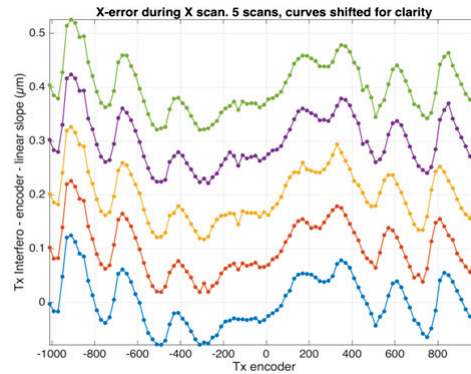


Figure 8: X-axis motion errors during X-axis sample stage scans; 5 scans were done in the range of  $2\text{mm}$ , each graph has been vertically shifted for clarity.

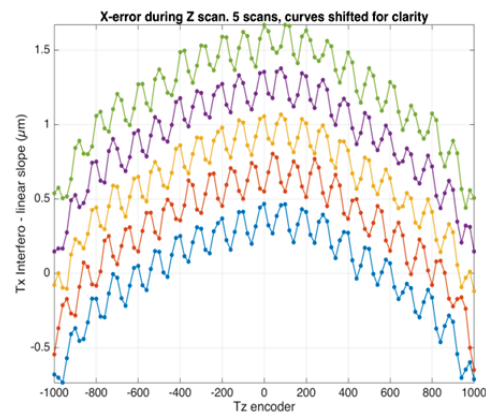


Figure 9: X-axis motion errors during Z-axis sample stage scans; 5 scans were done in the range of  $2\text{mm}$ , each graph has been vertically shifted for clarity

To properly characterize rotational motion errors, it was necessary to develop a method to characterize rotation stages using interferometry [1] [2] and separating reflector surface errors from rotation stage movement errors. Figure 10 shows the XYZ-parasitic errors during 30 full rotations with closed-loop control activated on the encoder. One can see that, even though the XYZ- errors are in the  $\mu\text{m}$ - range, the errors are repeatable to a band of a few hundreds of nanometers making it viable to approach 1 and 2 in subsection *Sample Stage Control*.

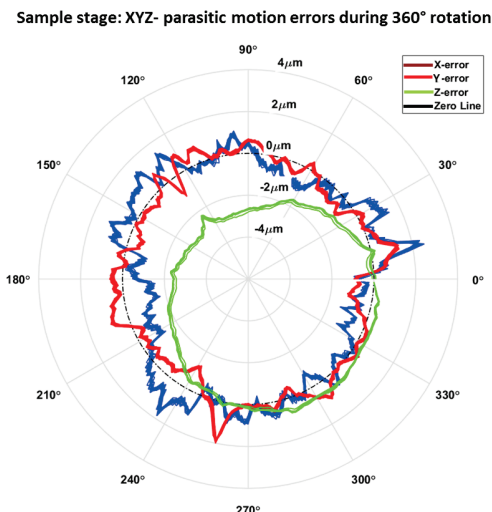


Figure 10: Sample stage, XYZ- parasitic error motions during full  $360^\circ$  rotations (30 rotations, 256 points of data per rotation).

### Sample Stage, 2D Scans

2D-scans in the XZ-plane were performed and tested using the sample stage setup depicted in Fig. 3 with the different modes of control available in Fig. 4. The scan area was over  $1 \times 1 \mu\text{m}$  of which the X-axis performed continuous Flyscans and the Z-axis stepscans with  $10 \text{ nm}$  steps. The sample holder reflector (#6 in Fig. 3) was in this case cubic in shape.

The first scan, see Fig. 11A, was performed without using interferometry feedback or compensation, which is to say that the XZ-linear drives were only driven in closed-loop control with their respective encoders. We can see here that the FWHM errors on the X-Axis was  $13.9 \text{ nm}$ . In the second scan, see Fig. 11B, the repeatable errors on the X-axis had been mapped using interferometry and were being corrected for in a feedforward manner using compensation tables reducing the FWHM errors on the X-Axis to  $9.07 \text{ nm}$  (no compensation on the Z-Axis in this case). Finally, in Fig. 11C, full interferometry feedback on the XZ- axes were used thus reducing the FWHM errors on the X-axis to  $8.19 \text{ nm}$  and  $2.79 \text{ nm}$  on the Z-axis.

### Sample Stage, $360^\circ$ Rotation Scans

Rotational scans on the Rz-axis were performed using the setup depicted in Fig. 3 with the control schemes available in Fig. 4, and with a cylindrical sample holder reflector (#6 in Fig. 3). Figure 12A shows the XY movement errors without interferometry feedforward or feedback compensation. From thirty full rotations, 90% of the radial errors held within  $1.25 \mu\text{m}$ . The repeatable errors were then mapped and corrected with feedforward compensation tables, see Fig. 12B, where the radial errors were drastically reduced to  $0.17 \mu\text{m}$ . By activating interferometry feedback correction on the XY-axes using two interferometer channels, as well as feedforward position compensation against reflector imperfections, the radial errors were further reduced to  $42 \text{ nm}$ , see Fig. 13.

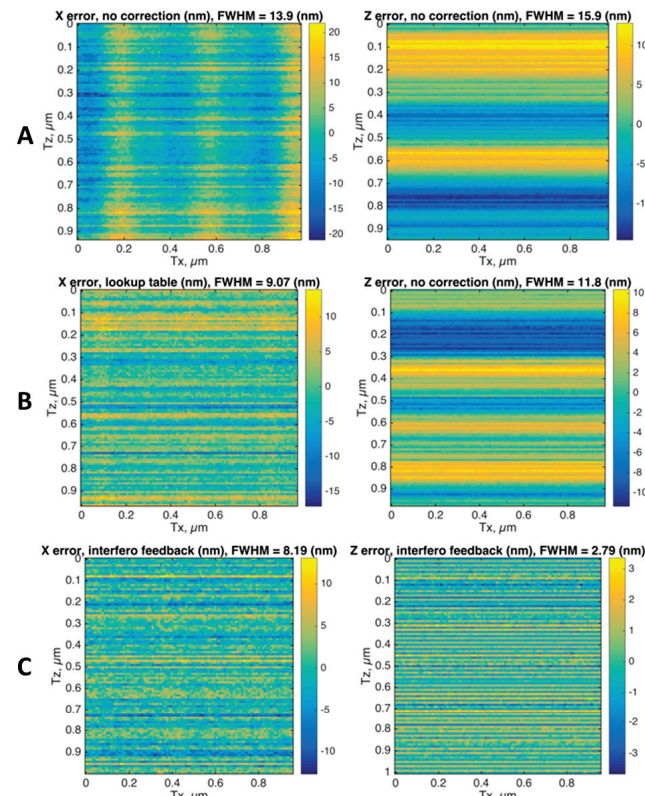


Figure 11: Positioning errors during  $1 \times 1 \mu\text{m}$  scan. X-axis was moving in a continuous motion while Z-movements were done in steps of  $10 \text{ nm}$ . (A) Scans without parasitic error compensation, however all actuators were run in closed-loop with their respective encoders. (B) Scans with error compensation on the repeatable errors of X-axis drive (feedforward compensation), all actuators were also run in closed-loop with their respective encoders. (C) Scans with XZ- error compensation using interferometric feedback, all actuators were also run in closed-loop with their respective encoders.

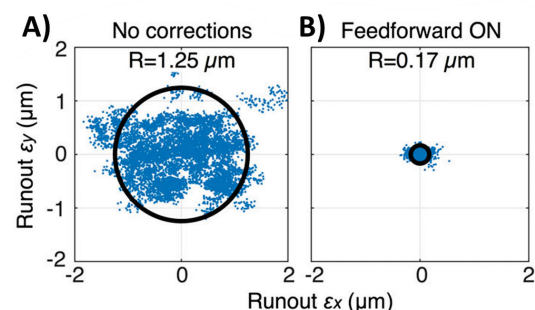


Figure 12: (A) Distribution of XY-runout without any active correction on the parasitic movements caused by the rotational drive. Measured for 30 full rotations with 256 steps per rotation, the radius of the 90% circle of confusion was  $1.25 \mu\text{m}$ . (B) Distribution of XY-runout with active feed-forward correction on the repeatable parasitic movements caused by the rotational drive. Measured for 10 full rotations with 256 steps per rotation, the radius of the 90% circle of confusion was  $0.17 \mu\text{m}$ .

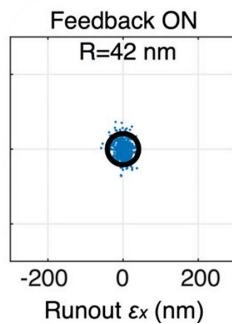


Figure 13: Distribution of XY-runout with active interferometry feedback correction on parasitic movements caused by the rotational drive, coupled with position compensation on the reflector surface errors. Measured for 2 full rotations with 256 steps per rotation, the radius of the 90% circle of confusion is 42nm.

### FZP Stage, Long-term Active Stabilization

Using the active stabilization control-loop as seen in Fig. 6, the FZP stage was set to stabilize a position in the XZ-plane over 11 hours with a correction-frequency of  $\sim 1\text{Hz}$  using interferometry as feedback. Figure 14 shows the long term position error histogram where one can see that thermal drifts were corrected and therefore reaching FZP position stability of (90%) 5.11nm. Tilt deviations did not exceed  $0.5\mu\text{rad}$  during the 11 hours of data capturing.

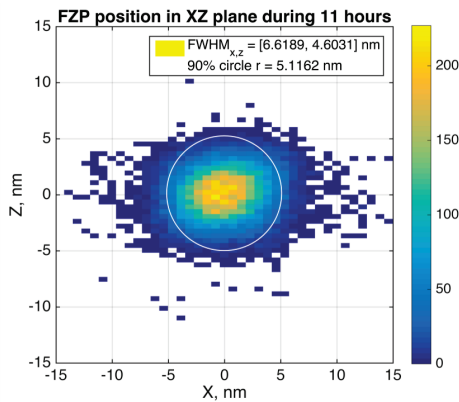


Figure 14: 2D histogram of the FZP positioning errors during 11 hours. The FWHM was found to be 6.6nm on the X-axis and 4.6nm on the Z-axis. The system keeps within 5.1nm in 90% of the time.

### Stability Between FZP and Sample Position

Mounting an image grating on the FZP stage and another one on the sample stage, stability measurements were conducted using a moiré method [9]; a metrology technique that utilizes the moiré effect with two overlapping repetitive structures. This method determined positioning stability between the sample and FZP along the XY-plane, see Fig. 15 for the setup.

Figures 16 and 17 show the measured stability between the two mounted stages; Fig. 16A shows that the holding stability (while all positioner drives were active in closed-

loop control) held within  $\pm 5\text{nm}$  peak-to-peak over the course of 0.6s. Running a 10nm pyramid step-scan on the X-axis, see Fig. 16B, while observing on the Y-axis revealed a quasi-perfect decoupling between the axes as the Y-axis movements held within  $\pm 5\text{nm}$ . Long-term 10-hour stability can be seen in Fig. 17: as the temperature drifted  $\sim 60\text{mK}$  the sample-FZP distance on the X-axis moved an equivalent of  $\sim 100\text{nm}$ .

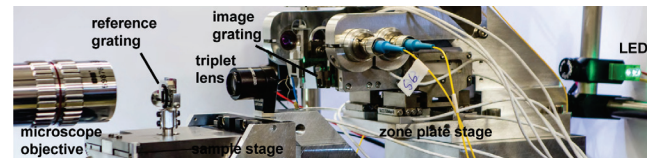


Figure 15: Photograph of the moiré setup with the sample- and FZP- stage.

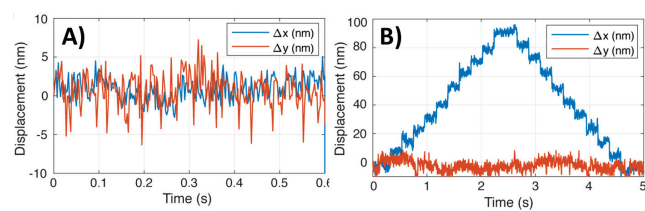


Figure 16: Moiré method results. (A) Steady-state vibrations in the XY-plane. Vibration-level found to be  $\pm 5\text{nm}$  peak-to-peak with a measurement frequency of  $40\text{Hz}$ . (B) Sample stage performing a 10nm pyramid step scan on the X-Axis. Little to no parasitic movements are seen on the Y-axis.

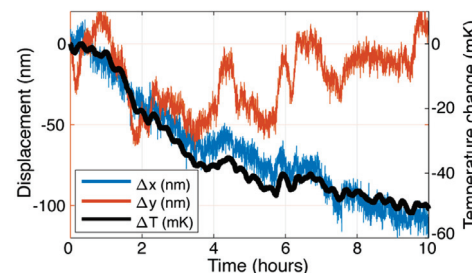


Figure 17: Long term thermal drifts measured during 10 hours correlate along the X-axis with changes of the ambient temperature by 60 mK.

## CONCLUSION

The FZP- and sample stage of an endstation prototype were constructed, tested, and characterized within the scope of the project. The system environment was built to have a very high thermal impedance with very low thermal drifts which was ultimately measured and verified to be within  $10\text{mK}$  ( $\sim 10\text{nm}$ ) over 8 hours.

### Sample Stage

Motion errors, in-axis as well as parasitic, were evident with all sample stage linear and rotational drives. As such, it became essential to separate repeatable from non-repeatable errors and incorporate these into different control schemes

(see subsection *Sample Stage Control*). Sample stage linear drives were characterized using interferometry then implemented in the different control schemes for comparison in 2D- scans. Similarly, the sample stage rotational drive was characterized using a new method [1] [2] determining its viability for the 2 control schemes.

Obtained results (see Figs. 18 and 19) show that feed-forward compensation tables were not only effective but in some cases the *minimum* requirement in terms of advanced control to achieve nanometric positioning: when doing small XZ 2D-scans, the X-errors during X-scans were reduced by  $\sim 34.7\%$  and the rotational drive had its radial motion errors reduced by  $\sim 86.4\%$ . Best results were however obtained using interferometry feedback control: X-errors in X-scans were reduced by  $\sim 41\%$ , Z-errors in Z-scans by  $\sim 82\%$ , and radial error motions from Rz by as much as  $\sim 96\%$ .

Even though interferometry feedback control outperforms the alternatives (see Figs. 18 and 19), there are sample range limitations when interferometry beam-loss occurs: ex. with a 10mm diameter cylindrical reflector (#6 in Fig. 3), effective XY lateral range can be  $\sim 400 - 500 \mu m$  before beam-loss occurs. Best results would be obtained by using interferometry feedback for a specified range and feedforward compensation tables when interferometry feedback is out-of-range.

It should also be noted that achieved results found in Fig. 11C were pushing the upper limits (issues with position synchronization between lines of data) of the SOLEIL data acquisition system and might get better results with the upcoming Soleil/Diamond PandABox system [10].

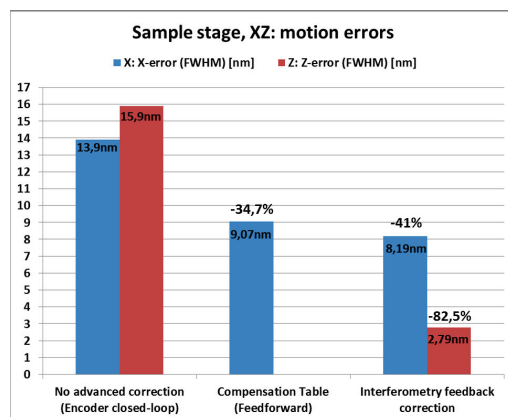


Figure 18: Sample stage XZ- motion errors FWHM results using the different modes of control (data taken from Fig. 11). Note that no feedforward compensation table correction was implemented for the Z-axis as it didn't have notable repeatable errors.

### FZP and Sample-FZP Stability

Interferometry feedback control, also used in the FZP stage, achieved position stability of  $5.11 nm$  (see Fig. 14) over an 11-hour time period. In addition, sample-FZP stability was determined using a new moiré method [9] where holding stability over the course of 0.6s was determined to

Sample stage, Rz: Circle of confusion (90%) [nm]

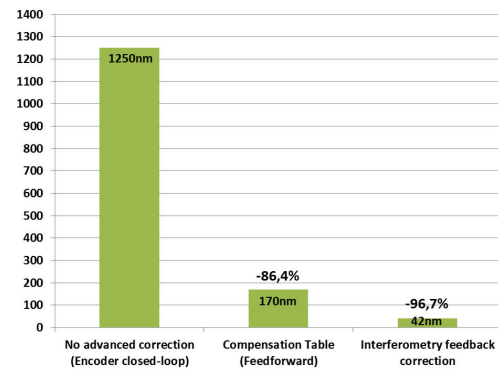


Figure 19: Sample stage circle of confusion (radius of 90%, in nm) using the different modes of control (data taken from Figs. 12 and 13).

be  $\pm 5 nm$  (See Fig. 16A), small pyramid X- step-scans show axis decoupling on Y (See Fig. 16B), and long term (10 hours) stability of  $\sim 100 nm$  (See Fig. 17).

## REFERENCES

- [1] T. Stankevič *et al.*, "Interferometric characterization of rotation stages for X-ray nanotomography", in *Review of Scientific Instruments* 88, 053703 (2017); doi: 10.1063/1.4983405.
- [2] S. Kubsky *et al.*, "Method and device for the three-dimensional characterisation of a surface of an object", in *WO Patent App. PCT/EP2015/074,011* (2016).
- [3] S. Zhang *et al.*, "Revolution Project: Progress in the Evolution of Soleil Motion Control Model", in *Proc. of the 15th Int. Conf. on Accelerator and Large Experimental Physics Control Systems (ICALEPCS'15)*, Melbourne, Australia, Oct. 2015, pp. 201–204.
- [4] Delta Tau, <http://www.deltatau.com>
- [5] A. Somogyi *et al.*, "Status of the Nanoscopium Scanning Hard X-ray Nanoprobe Beamline of Synchrotron Soleil", in *Proc. of the 11th International Conference on X-ray Microscopy*, Shanghai, China.
- [6] U. Johansson *et al.*, "NanoMAX: A hard x-ray nanoprobe beamline at MAX IV", in *Proc. of SPIE*, Vol. 8851 88510L-9.
- [7] N. Leclercq *et al.*, "Flyscan: A fast and multi-technique data acquisition platform for the SOLEIL beamlines", in *Proc. of the 15th of International Conference on Accelerator & Large Experimental Physics Control Systems (ICALEPCS'15)*, Melbourne, Australia, Oct. 2015, pp. 826-829.
- [8] Galil, <http://galilmc.com/>
- [9] U. Vogt *et al.*, "Moiré method for nanometer instability investigation of scanning hard x-ray microscopes", in *Opt. Express* 25, 12188-12194 (2017).
- [10] S. Zhang *et al.*, "PandABox: A Multipurpose Platform For Multi-technique Scanning and Feedback Applications", presented at the 16th Int. Conf. on Accelerator and Large Experimental Physics Control Systems (ICALEPCS'17), Barcelona, Spain, Oct. 2017.